Impact of channel geometry on two-phase flow in fuel cell microchannels

Julie E. Steinbrenner[*], Eon Soo Lee[1], Carlos H. Hidrovo[2], John K. Eaton, Kenneth E. Goodson

Stanford University, Department of Mechanical Engineering, 440 Escondido Mall, Building 530, Room 224, Stanford, CA 94305 USA

ABSTRACT

An important function of the gas delivery channels in PEM fuel cells is the evacuation of water at the cathode. The resulting two-phase flow impedes reactant transport and causes parasitic losses. There is a need for research on two-phase flow in channels in which the phase fraction varies along the flow direction as in operating fuel cells. This work studies two-phase flow in 60 cm long channels with distributed water injection through a porous GDL wall to examine the physics of flows relevant to fuel cells. Flow regime maps based on local gas and liquid flow rates are constructed for experimental conditions corresponding to current densities between 0.5 and 2 A cm^{-2} and stoichiometric coefficients from 1 to 4. Flow structures transition along the length of the channel. Stratified flow occurs at high liquid flow rates, while intermittent slug flow occurs at low liquid flow rates. The prevalence of stratified flow in these serpentine channels is discussed in relation to water removal mechanisms in the cathode channels of PEM fuel cells. Corners facilitate formation of liquid films in the channel, but may reduce the water-evacuation capability. This analysis informs design guidelines for gas delivery microchannels for fuel cells.

© 2011 Elsevier B.V. All rights reserved.

1. Introduction

The management of water in a proton exchange membrane (PEM) fuel cell is a performance-limiting concern in these carbon-dioxide-free energy-conversion devices. While the performance of the membrane depends on ample humidification, liquid water in the microporous layer, gas diffusion layer (GDL), and/or gas delivery channels impedes the flow of reactant gases to catalyst sites and cripples cathodic reaction rates. Two-phase flow phenomena have been identified as concerns for flooding-induced performance degradation, cell voltage hysteresis, increased parasitic pumping losses, and the absence of predicted performance improvements [1–4]. While microchannels are proposed for use in PEM fuel cells with promised benefits of increased convective transport, flexibility of geometric design, and decreased resistive path lengths, these benefits have not been realized in practical systems [3]. One explanation for the unrealized performance improvements is an increased propensity toward flooding in smaller channels where surface tension force becomes significant compared with viscous, inertial, and pressure forces. There is a need for studies that consider two-phase flow in microchannel geometries that mimic conditions in fuel cell channels, where long channel lengths, distributed water introduction, and porous walls are defining characteristics. The present work uses experimental methods to study the physics of two-phase flow in geometries common to practical fuel cells which is critical to their performance.

Some two-phase flow characterization tools have been developed for in situ fuel cell applications [5,6]. In fuel cell components lacking optical access, neutron imaging, magnetic resonance imaging, and X-ray tomography allow for identification of liquid water through opaque surfaces. Neutron imaging is a promising technique for real-time imaging of liquid water in an operating fuel cell [7–11]. This technique is limited to two dimensions. Detailed analysis is necessary to distinguish flow structures between the anode and cathode. X-ray tomography and magnetic resonance imaging have been used to create three dimensional maps of the water concentration in the membrane and GDL layers with limited resolution [12,13].

Opaque bipolar plates, layers of porous materials with various surface properties, and non-uniformity of water production rate and location complicate the imaging and analysis of flow regimes in fuel cell channels. Yet fuel cells with modified geometries allow optical access into the gas distribution channels [14–21]. These cells have been used to correlate the appearance of liquid water with increases in gas pressure in the channels and voltage drops in the fuel cell. The setup may interfere with typical reaction distribution because the electrical pathways are distorted when conductive bipolar plates are replaced with non-conductive glass plates for

* Corresponding author. Tel.: +1 650 823 0592; fax: +1 650 723 7657.
E-mail addresses: julie.steinbrenner@stanford.edu (J.E. Steinbrenner), hidrovo@mail.utexas.edu (C.H. Hidrovo), goodson@stanford.edu (J.K. Eaton), eatonj@stanford.edu (K.E. Goodson).
[1] Present address: Advanced Materials Lab, Corporate R&D Institute, Samsung Electro Mechanics, 314 Maetan-dong, Youngtong-gu, Suwon, Kyunggi-do 443-743, Korea.
[2] Present address: The University of Texas at Austin, Mechanical Engineering Department, ETC 7.148A, 1 University Station C2200, Austin, TX 78712-0292, USA.

Nomenclature

i	current density/A cm^{-2}
α	osmotic drag coefficient
Q	volumetric flow rate/L min^{-1}
U	superficial velocity/m s^{-1}
λ	stoichiometric ratio
W	channel width/m
L	channel length/m
F	Faraday's constant/C
M	molar mass/g mol^{-1}
ρ	density/kg m^{-3}

Subscripts

a	air (gas phase)
w	water (liquid phase)

optical access. While much insight can be drawn from these studies in the correlation between liquid water and fuel cell performance, the precise flow conditions at any particular location in the cell are difficult to quantify due to non-uniformities in reaction distribution and subsequent uncertainties in local flow rates.

Comparison of in situ and ex situ experimental results is complicated by the definitions commonly prescribed in the literature for given operating conditions. A single stoichiometric ratio is often reported, but in reality the air flow rate is held at a fixed value and the current density or cell load is swept through a range of operating conditions. Therefore, the reported stoichiometric ratio is valid at only a particular representative current density. This procedure allows for similar fluidic conditions in each case however, the electrochemical activity and species concentration profile along the channel varies as more or fewer reactants are consumed. Despite these difficulties, ex situ experiments offer the advantage of greater control of experimental conditions. Absent the electrochemistry of an operating fuel cell, these setups allow observation of the two-phase flow characteristics in fuel cell geometries while quantifying the local flow rates of both phases.

Various geometric configurations have been employed which simulate the conditions of a fuel cell in an ex situ visualization experiment. Lu et al. [22] and Zhang et al. [23] constructed parallel flow channel systems with gas and liquid injection relevant to fuel cell conditions. Su et al. studied flow in 5 mm square cathode channels by injecting water into the channels through a carbon paper layer from a single liquid reservoir [24]. Others have examined droplet departure from a GDL into a gas channel using short channel segments [25,26]. Few experimental studies have considered fuel cell flow conditions in microchannels, which is significant as two-phase flow transitions are commonly considered to be functions of the superficial velocity of the phases. While flow rates in fuel cell channels are fixed by the current density and stoichiometry, flow velocities are then determined by channel dimensions.

Experimental studies for lab-on-a-chip and microchannel cooling applications characterize two-phase flow patterns in microchannels [27–31], however these studies do not replicate the distributed liquid water introduction, long channel lengths, and porous boundary conditions of a PEM fuel cell. Additionally, the liquid flow rates of interest for these applications are much higher than those relevant to fuel cell operation. Pehlivan et al. provide a review of the two-phase flow regimes observed in mini channels as small as 800 μm [32]. His universal flow regime map based on experimental results from the literature does not extend to low water flow rates relevant for fuel cell channels. Nevertheless, air flow rate is the dominant parameter influencing flow regime tran-

sitions at the lowest reported water flow rates, a result which may be relevant for the lower water flow rates applicable to fuel cells.

The present work bridges the gap between in situ experiments on operating fuel cells and two-phase flow experiments in different geometries. Liquid water is introduced into the channel through the porous carbon paper gas diffusion layer which flanks one channel wall, thereby allowing for the characterization of flow regime transitions with known flow rates. Unlike visualization of operating fuel cells, this setup allows for precise control of both liquid and gas flow rates and injection conditions. Compared with other ex situ experiments, this study incorporates channels with smaller cross-sectional dimensions than many previous fuel cell related studies. Compared with fundamental two-phase flow studies in microchannels, this study better replicates the characteristics of fuel cell channels, including longer channel lengths and distributed water introduction. The channel dimensions of 500 μm × 500 μm square channels were chosen as a trade-off between the projected performance improvements of microchannels and expected issues with flooding and clogging in small channels. Understanding the flow regimes in these channels, which are smaller in dimension and cross-sectional area than standard fuel cell channels, provides insight into the possible use of microchannels for fuel cell applications. The smaller separation between channel walls means that a larger percentage of the droplets entering the channel will come in contact with a channel wall, potentially leading to more favorable flow regimes at the expense of larger viscous losses. This study provides insight to key two-phase flow structure transitions of importance for performance-critical water management in PEM fuel cell channels.

2. Experimental methods

2.1. Sample geometry and preparation

A single serpentine channel replicates flow conditions associated with fuel cell gas delivery channels as shown in Fig. 1. A channel with a 500 μm × 500 μm square cross-section is machined in acrylic. The channel follows a 60-cm long serpentine layout incorporating five long segments and four short turns. The fourth wall of the channel is comprised of a 2 mm wide, 190 μm thick ribbon of porous carbon paper GDL which follows the channel geometry and fits into a latex gasket which is carefully patterned using a CO_2 laser ablator. The GDL paper is pressed against the channel structure with an acrylic slab using 44 evenly spaced bolts for even distribution of pressure. Water is injected into the channel at eight locations using a multi-syringe pump (Harvard Instruments) via 500 μm diameter holes through the bottom acrylic slab on the backside of the carbon paper wall, causing water flow through the GDL into the channel.

Various injection configurations were considered before discrete liquid injection was chosen. While an ex situ setup does not perfectly replicate the molecule-by-molecule production of water of operating fuel cells, visualization of operating fuel cells shows the water entering the channel in the form of droplets (e.g. [27]). The approximation of water introduction from discrete points still provides some insight into the overall flow behavior once the water has entered the channel. Other ex situ injection geometries incorporating reservoirs or channels behind the GDL layer suffered from the preferential flow of air through the GDL pores and small channels. In these geometries, liquid water cannot be made to completely fill injection reservoirs when a pressure gradient is applied across the device; air is unavoidably entrained into these cavities and flows through the channels and the injection reservoirs in parallel. Consequently, liquid injection was very unevenly distributed and local conditions were difficult to characterize. Compared with reservoir or channel injection, the discrete injection scheme provides control

Table 1
Experimental conditions and fuel cell equivalents for serpentine channels.

i (A cm^{-2})	Q_w (μL min^{-1})	Q_w/inj. (μL min^{-1})	Q_a/std. (L min^{-1})			
			Stoich. coeff.			
			1	2	3	4
0.5	33.6	4.21	0.088	0.176	0.264	0.352
1	67.3	8.41	0.176	0.352	0.528	0.704
2	134.6	16.83	0.352	0.704		

of the local water flow rate and facilitates observation of changes in the flow structure as more water is introduced as the two-phase flow progresses downstream.

The channels were carefully polished with plastic polishing compound (Novus). In order to examine the influence of corners on the flow regime transitions, samples with 11 cm long straight channels are also constructed. These channels are similarly milled in acrylic, with eight water injection locations evenly spaced along the length.

Toray GDL papers (TGPH-090) with and without impregnation with a 10 wt% Teflon solution are used in order to examine the effect of GDL hydrophobic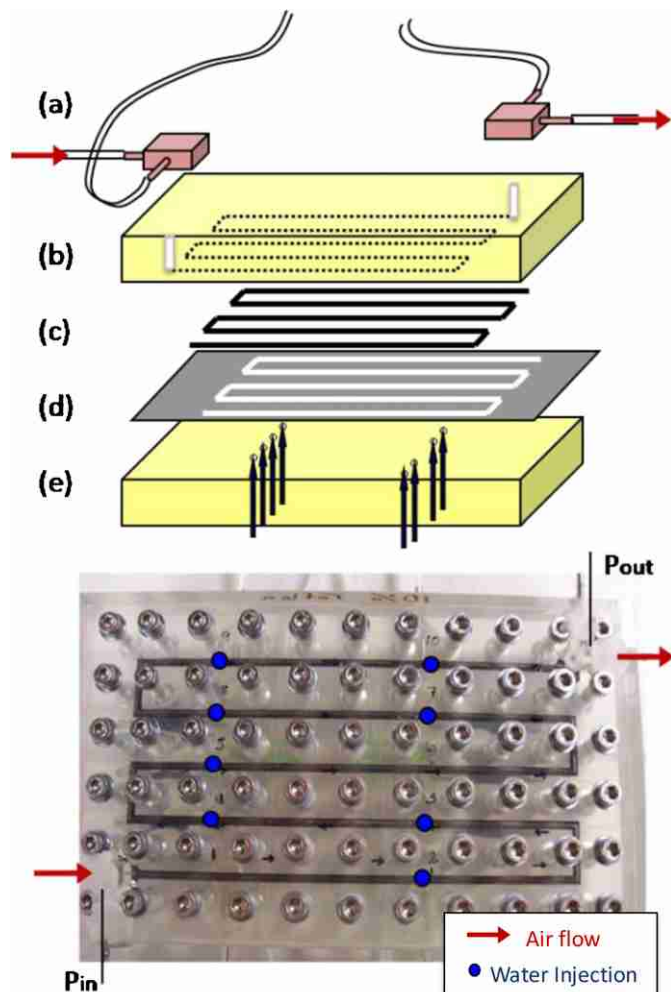ity on the flow observed in the channels. Toray GDL paper is a commercially available material commonly used in fuel cell manufacture. The specific formula for hydrophobic coatings is proprietary and varies significantly from manufacturer to manufacturer. The use of this teflonated GDL is intended to provide qualitative evidence of the influence of hydrophobicity of the porous material on the flow in the channels.

2.2. Procedure

Fig. 2 shows the experimental setup delivering air and water to the channel structure. Air and water flow rates are chosen according to the operating conditions of a PEM fuel cell. Upstream air pressure is held constant at a gage pressure of 1 atm. Downstream pressure is regulated with a needle valve at the exit in order to establish the desired flow conditions. Inlet and differential pressures are measured using diaphragm differential pressure sensors (Validyne). Air flow rate is measured with flow meters located in-line upstream of the test section (Sensirion thermal mass flow meter and Omega laminar-passage air flow meter). Liquid injection is metered with a syringe pump (Harvard PHD 2200) fitted with a multiple syringe rack holding eight identical glass syringes (Hamilton Gastight 1 mL). Care was taken to evacuate all syringes, tubing, filters, and connectors of air bubbles to reduce the capacitance of the system. Hard-walled Teflon tubing was used for the same reason.

Experimental parameters correspond to reasonable operating conditions for PEM fuel cells as enumerated in Table 1. Water is injected at rates equivalent to current densities, i, between 0.5 and 2 A cm^{-2}. The equivalencies are calculated according to Eqs. (1) and (2), assuming an osmotic drag coefficient, α, of 0.5 molecules of water per proton and an effective land area equal to the channel area. Air flow rates correspond to equivalent stoichiometric ratios, λ, from 1 to 4.

$$Q_{water} = i \cdot \frac{(1+\alpha)}{2F} \frac{M_{H_2O}}{\rho_{H_2O}} \cdot (2 \cdot W \cdot L) \qquad (1)$$

$$Q_{air} = i \cdot \frac{(2 \cdot W \cdot L)}{0.21 \cdot F} \frac{M_{air}}{\rho_{air}} \lambda \qquad (2)$$

Between experiments, dry air flows through the channel for at least 30 min to provide consistent starting conditions by drying the GDL of accumulated water from the previous test. The air used in these experiments is dry and at room temperature air, since the ex situ setup is less sensitive to the effects of temperature and hydration on reaction rates and fuel cell performance of an operating fuel cell. The air flow rate is established by setting the downstream needle valve. Then liquid water injection begins. Pressure and air flow rates are recorded while images of the channel are captured using a 1392 × 1040 pixel CCD camera (Nikon Coolsnap ES) once flow conditions appear steady after several minutes. Two hundred images are collected sequentially to create movies of the flow in the channel. The data and image collection is repeated after 10–15 min of flow to ensure that flow conditions are not changing.
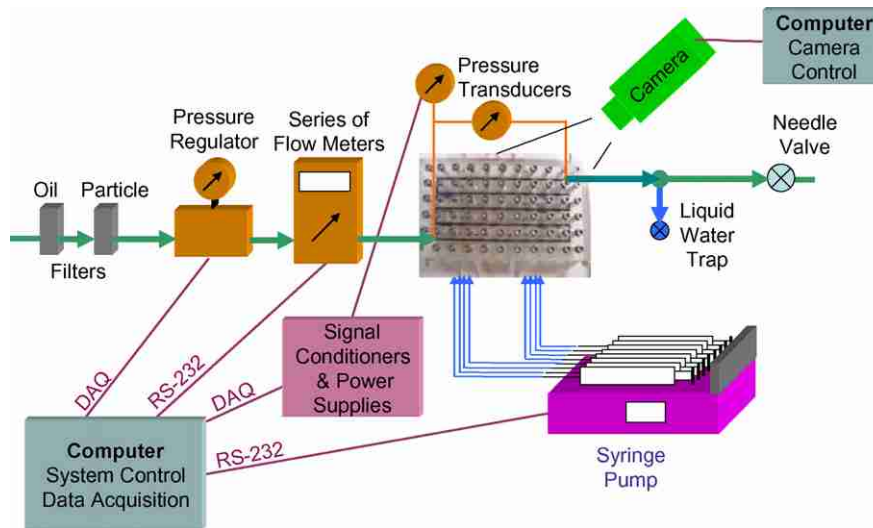

Fig. 1. Channel assembly. The following layers are sandwiched together to create a sealed serpentine channel with distributed water injection through the porous GDL layer: (a) connections to air tubing and pressure transducers, (b) 1/4″ cast acrylic with 500 μm × 500 μm × 60 cm channel, (c) 190 μm thick × 2 mm wide Toray Carbon Paper GDL (0 or 10 wt% Teflon), (d) latex gasket, (e) 1/4″ thick cast acrylic with 300–500 μm diameter water injection holes.

Fig. 2. Schematic of experimental setup.

2.3. Flow visualization

The entire channel is visualized in several images by moving the flow structure with respect to the camera, which is fitted with a macrophotography lens. For the serpentine channels, eight separate sets of images are collected. Images are decomposed into channel segments, as illustrated in Fig. 3, in order to examine the flow as it progresses along the length of the channel.

For analysis of the flow regimes, the flow structure in each channel segment was examined and categorized. Fig. 4 shows representative images of the flow structures that were observed in the channels. Stratified flow is steady and the position of the interface does not vary with time for given operating conditions, while plug and slug flow show transient variation of the gas–liquid–solid interfaces. Wavy flow has a constant liquid–solid interface at the channel wall, but a varying liquid–gas interface. For fluidic analysis, local air and water flow rates are calculated along the channel based on the inlet air flow rate and the total quantity of water injected upstream of the imaging location, such that at one test condition, there is a single air flow rate but eight local water flow rates due to the eight water injection locations.

3. Results and discussion

3.1. General trends

Measurements and images are analyzed to characterize the system performance, channel characteristics, and two-phase flow structures. The channels are characterized using the pressure drop and flow rate measurements. Images of the channel under various operating conditions are analyzed to evaluate the evolution of the two-phase flow structure.

The straight and serpentine channels exhibited similar viscous losses as shown in Fig. 5. Here the average pressure gradient is
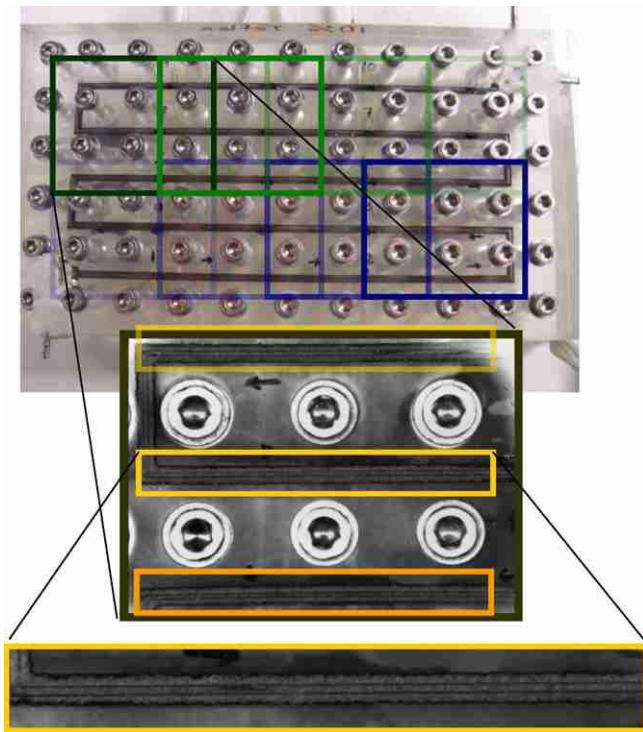

Fig. 3. Image decomposition. (a) The entire channel imaged at high demagnification, (b) one of the eight images of the channels, and (c) one channel segment extracted from an image.
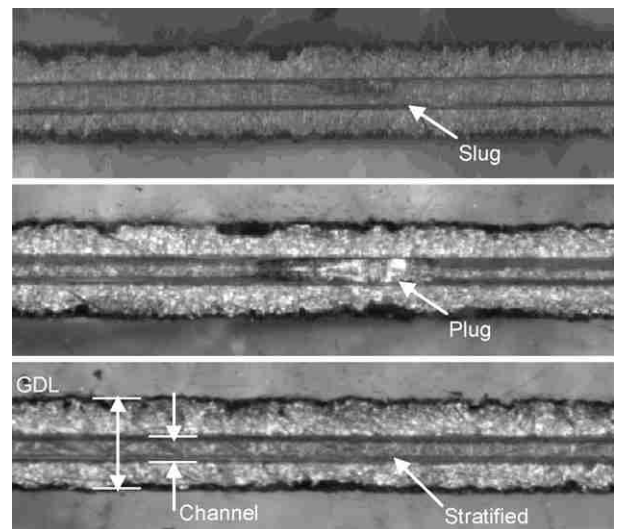

Fig. 4. Representative images of two-phase flow structures: (a) slug, (b) plug, and (c) stratified.
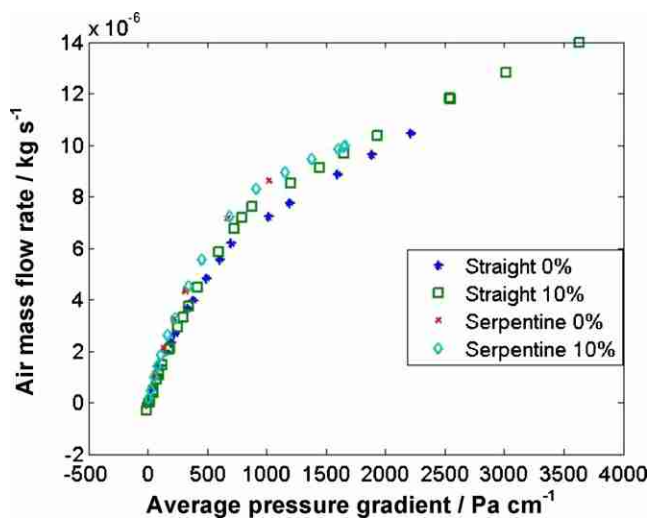
Fig. 5. Viscous losses in straight and serpentine channels with no water injection. Samples with non-teflonated GDL (0%) and teflonated GDL (10%) show similar behavior.

Fig. 6. Observed flow structures and general evolution of flow regimes.

defined as the total pressure drop divided by the length of the channel (60 cm for the serpentine channel, 11 cm for the straight channel). Gas pressure is measured at the inlet and the outlet of the channel. There was no significant difference in the pressure vs. flow rate curves between the two types of GDL tested. The similarity in the viscous loss curves for serpentine and straight channels indicates that minor losses due to the 90° corners are not significant. The non-linear relationship between pressure drop and air flow rate indicates that density changes cannot be neglected. However, a variable density relationship using the ideal gas law significantly under predicts the air flow rate for a given pressure drop. Air flow through the gas diffusion layer flanking the channel partially explains this discrepancy. Water introduction caused a very slight decrease in flow rate for a given pressure drop (compared to a dry channel) for both samples.

The flow structure is examined along the length of the channel for each operating condition. As expected, the structure of the liquid water depends upon the properties of the channel wall, the amount of water in the channel, the air flow rate, and to some extent, the distribution of water injection. While there are general trends in the progression of flow regimes and the conditions under which they are observed, a strong stochastic element exists due to the complicated fluidic interactions in the serpentine geometry with a textured, porous wall and non-uniform surface properties. More water is seen in the channels of the structures assembled with GDL containing Teflon. This difference may result from variations in flow structure and liquid water velocity in the channels or may indicate that more liquid water flows through the hydrophilic GDL so that less water is forced into the channels.

Fig. 6 provides a qualitative overview of flow structure observations according to air and liquid flow conditions. The horizontal axis corresponds to a progression along the channel and a corresponding increase in local water flow rate as additional liquid injection locations are encountered. The upper and lower branches represent flow structures occurring under relatively higher and lower air flow conditions. Black arrows between images represent common transitions between flow regimes as more liquid is encountered in the channel. The dry channel transitions to intermittent flow, a regime where water moves through the channel in discrete packets droplets, slugs, or plugs. Intermittent flow becomes wavy flow when the water travels down the channel as an abrupt thickening of a liquid film on the side walls of the channel. Finally, a stratified flow ensues when the sidewall film becomes steady and no
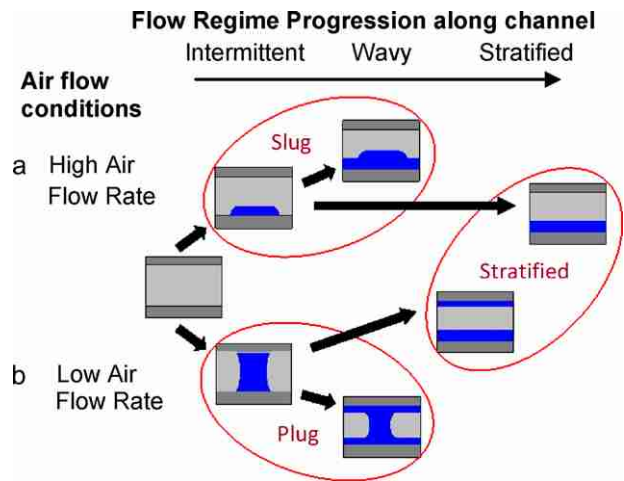
significant oscillations are observed at the interface. Stratified flow exists most commonly at the furthest downstream locations, while slug/plug flow is rarely observed downstream of the first several injection locations.

These trends suggest that stratified flow is hydro dynamically preferred to intermittent flow regimes, provided there is enough liquid flowing in the channel to maintain such a film. When a slug or plug travels, the three-phase interface moves so surface tension forces must be overcome. Once the liquid forms a film along a channel wall, this force is eliminated in the flow direction and the gas–liquid surface area is minimized. The water is propelled by the pressure gradient in the channel and shear forces from the air. A liquid film provides the most efficient means of water evacuation from the channels.

One of the most common transitions is a change in structure of stratified flow from occurrence on two channel walls to occurrence on a single wall. Several conditions facilitate this transition, including the presence of liquid resting on the GDL surface, a water injection point which also wets the GDL, or a corner. These liquid bridges may form where local variations in the surface properties of the GDL favor the accumulation of water. Fig. 7 shows two such transition points, both in a straight channel at an injection point (a) and at a corner (b).

Analytical solutions to the momentum equations for simplified stratified flow in a rectangular channel reveal the hydrodynamic advantage of single-wall stratified flow over two-walled stratified flow. The pressure gradient within a channel of a particular dimension is determined by the ratio of flow rates of air and liquid phases (which is proportional to the stoichiometric ratio) and scales with the absolute magnitude of the flow rate (proportional to current density). After non-dimensionalization, the ratio of pressure gradient to volume flow rate of air is a function of the ratio of water to air volume flow rate (equivalent to fuel cell stoichiometry) and aspect ratio of the channel. The pressure gradient necessary to sustain equivalent flow rates of both gas and liquid in identical square channels is between 4 and 15% lower for stratified flow on a single-wall compared with stratified flow on two walls. Additionally, a single wall stratified flow maintains half the interfacial area between phases, so surface energy is also minimized.

3.2. Comparison of flow conditions

There are several ways to compare the data between test conditions. A comparison of equivalent fuel cell operating conditions is interesting for direct application to fuel cell systems. The stoichiometric ratio fixes the ratio of air and water flow rates; an increase
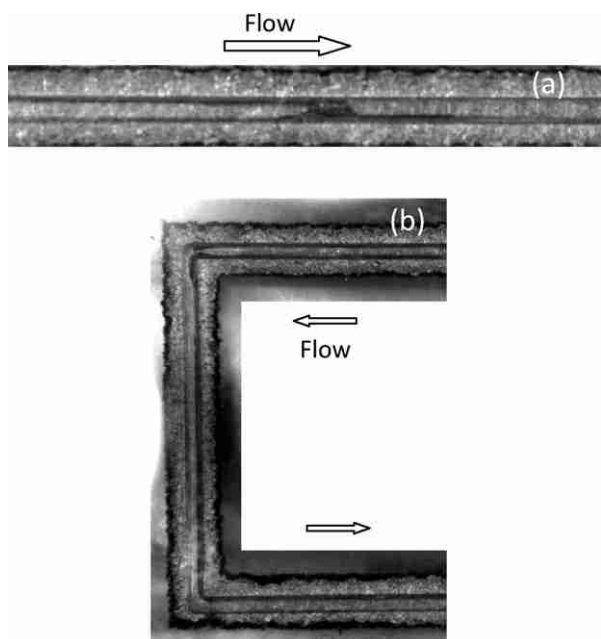
Fig. 7. Images of flow transitions: (a) transition of stratified flow from two-walls to one-wall, (b) transition of stratified flow from two-walls to one-wall at upper corner.

in current density for a fixed value of lambda increases both the air and water flow rates proportionally. A constant stoichiometric coefficient corresponds to a line with unity slope on a standard flow regime map with superficial velocities of gas and liquid on the x-and y-axes, respectively.

For channels with teflonated GDL, for a given current density, as the stoichiometric ratio (or air flow rate) increases, the transition from intermittent flow to films occurs later in the channel. As current density increases for equivalent stoichiometric ratios, the transition point occurs further upstream. Alternatively, insight can be gained by comparing equivalent fluidic conditions, where the air flow rate in the channel is held constant, but the water flow rate varies. This simulates the common situation where air flow rate is fixed, but local current density varies in response to the load applied to the cell. As current density increases for equivalent air flow rates, the transition point similarly occurs further upstream.

For non-teflonated channels, the trends are less consistent. For $i = 0.5\,A\,cm^{-2}$ and low air flow rates, water rests in the channel as thin films and as liquid droplets/plugs sitting on the GDL. When the air flow rate increases, slugs are observed and the transition to a film occurs halfway through the channel. For higher water flow rates, slugs are observed for the lower air flow rates and films are observed at high air flow rates. Films occur at highest water flow rates. For equivalent stoichiometric ratios, the trend is progression from thin films with stationary plugs on the GDL, to moving slugs, to films.

3.3. Variation of flow structure with flow rate

Most two-phase flow studies organize the flow regimes onto regime maps according to the superficial gas and liquid velocities. In this study, the distributed water introduction along the length of the channel requires that the flow regime map consider the local flow rate of liquid after each injection location. Consequently, each experimental condition provides information at eight aligned locations in flow rate space. Furthermore, in this complicated geometry, flow structures often change spatially between injection points,
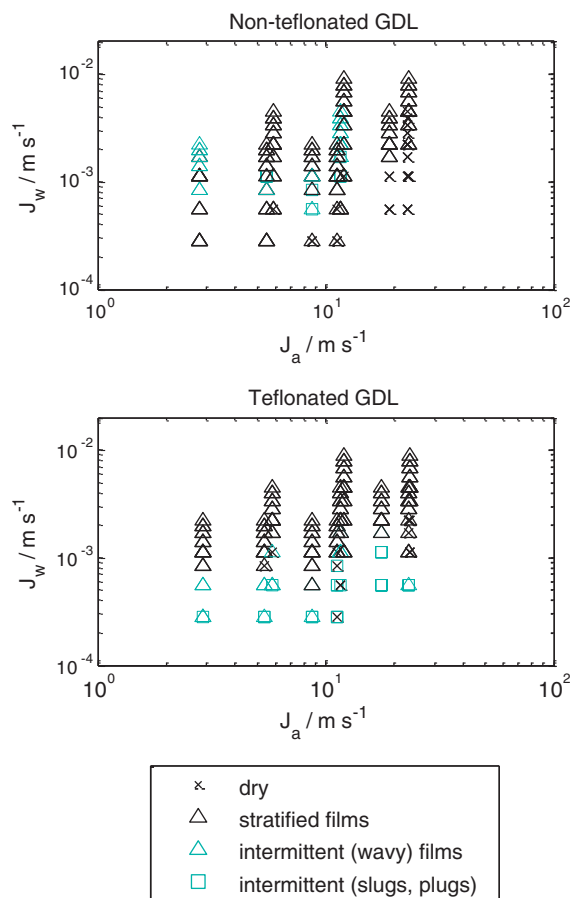

Fig. 8. Flow regimes in serpentine channels mapped against superficial air and water velocities. Black symbols represent stable flow regimes; gray symbols represent intermittent flow structures.

such that a single experimental condition may result in multiple flow regimes for a particular air and local water flow rate, depicted as overlapping points on the regime map. Fig. 8 shows observed flow regimes plotted against local air and water flow rates. The local water flow rate at a given position is the product of the number of liquid injection points upstream from the imaging location and the rate of water introduction per injection point. The volumetric air flow rate is determined from the inlet mass flow rate and pressure.

In the samples containing Teflon, intermittent (slug and plug) flow regimes occur for low water injection rates. This corresponds to the first several injection points along a channel. Plug flow occurs at low air flow rates, but slugs exist at the same flow parameters because these plugs are quickly broken into slugs as they travel down the channel. At higher air flow rates, low liquid flow rates yield slug flow. For all air flow rates, stratified flow is the dominant flow regime at high water flow rates.

The samples without Teflon also exhibit stratified flow at the highest liquid flow rates as well as at the highest air flow rates. Intermittent flows are observed at moderate liquid flow rates; plug flow occurs at only under the lowest air flow and slugs occur at moderate air flow. Comparing the regime maps for the serpentine samples, the intermittent regimes occur for higher water flow rates in the hydrophilic GDL case than in the hydrophobic GDL condition. This similarity supports the observation that more liquid water appears in the channels with Teflon coating. Liquid water preferentially flowing through the GDL in the hydrophilic case effectively lowers the water flow rate occurring in the channel.
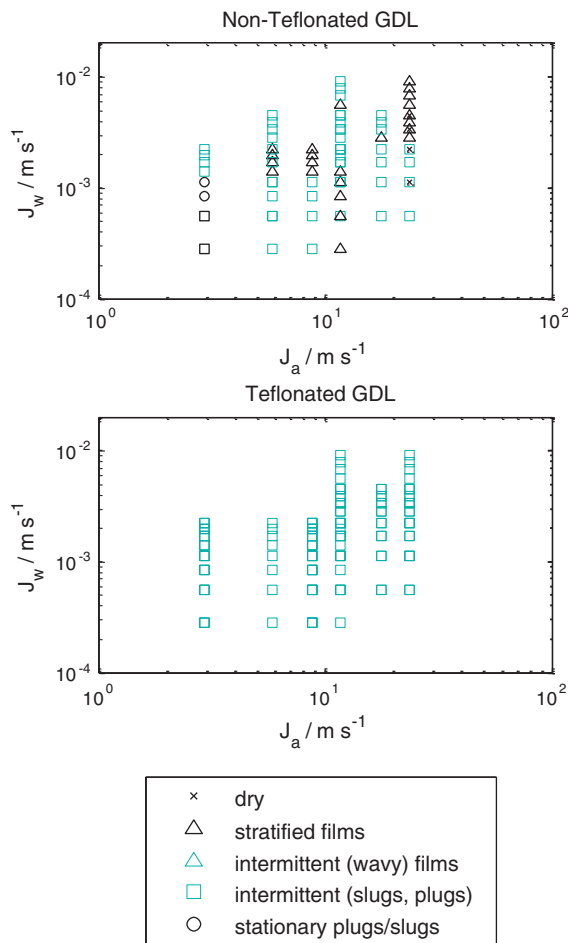
Fig. 9. Flow regime map for straight channels with equivalent flow rates to serpentine channel conditions of Fig. 8. Compared with the serpentine channels, the straight channel configuration tends toward intermittent flow regimes.

3.4. Effect of corners on flow regime evolution

Flow rates for the straight channels were chosen with two equivalencies to the serpentine channels: equivalent fuel cell operating parameters where flow rates are adjusted in proportion to the reduced area of the straight channel, and equivalent hydrodynamics where the flow rates of each phase are identical to the serpentine channel conditions. Matching fluidic conditions in the channels provide a control to examine the effect of the corners on the flow, while matching fuel cell conditions provide a better comparison for a fuel cell channel design which would include multiple shorter channels in parallel. This section describes the results of matching fluidic conditions. Section 3.5 describes the flow regimes which result from the same current density and stoichiometry in each channel.

For matching fluidic conditions, air and water are introduced into the straight channel at the same flow rates as for the serpentine channel, as given in Table 1. (This condition corresponds to much higher current densities which would not be practical. This particular analysis therefore relates only to the hydrodynamic effects of the corners on the flow regimes.) The pressure drop in the channel is proportionally smaller than that in a serpentine channel, so the average pressure gradient is comparable for these two channels and pressure forces exerted on droplets and films in the channels are equivalent.

Fig. 9 is a flow regime map for the straight channel experiments. In these channels, intermittent flow regimes were observed more

often than stratified films. In fact, stratified flow was not observed in the straight channel with teflonated GDL under any flow conditions.

Interestingly, flow regime transitions do not occur at the corner in the serpentine channel samples; however, the flow more frequently transitions to films when corners are present. The effect of the corner, therefore, is to facilitate the formation of films. Possible means for this effect are the build-up of water in the corners, which then facilitates the formation of films when there would otherwise not be enough liquid to sustain a film. When transitions occur at water injection locations, where they most often do, there could be a build-up of water in the GDL or corners of the channel near the injection point that creates conditions favorable to film formation. The corners reduce the water-repellent effect of the teflonated GDL sample by creating locations where water can accumulate and remain in the samples.

This effect is consistent, but less marked in the non-teflonated channels, where the conditions are inherently more favorable for water retention than in the teflonated samples. Unlike the teflonated samples, films and stationary water plugs are observed in the more hydrophilic non-teflonated samples. Films with plugs on the GDL occur at low air flow rates; moving slugs occur when air flow rates are increased. Finally, films occur at the highest air flow rates. These trends are similar to those observed in the serpentine channels, except that slugs are observed over a wider range of operating conditions, specifically for higher air flow rates.

3.5. Implications for fuel cell channel design

Matching fuel cell operating conditions in a short straight channel gives insight in the effect of length and design of multiple channels for fuel cell gas delivery channels. In these 11 cm samples, the flow rates in the straight channels are 82% lower than those in the serpentine channels, proportional to the reduction in length according to Eqs. (1) and (2). Flow rates for the straight channel samples with equivalent fuel cell operating conditions are listed in Table 2. The overall pressure drop and local pressure gradient is also smaller in these channels.

The reduction in pressure gradient and shear forces due to the reduced flow rates reduces the forces acting on the liquid in the channels. In both the samples with and without Teflon, slugs are stationary near the channel entrance for low air flow rates. Further downstream and after several water injection locations, motion of these slugs ensues. When air flow rates are increased, corresponding to higher stoichiometric ratios or current densities, moving slug flow dominates and water does not remain static in the channels. Slug detachment and its motion downstream is affected by the pressure gradient forces experienced by the liquid slug in the channel so that higher air flow rates create larger pressure forces on the slug [33]. In terms of fuel cell design, this suggests that the higher pressure gradients afforded by high air flow rates could facilitate the removal of liquid water from the gas channels, and multiple parallel segments which would reduce the local volumetric flow rates and overall system pressure drop might adversely impact water removal from the channels.

Most fuel cell system designs include multiple parallel straight or serpentine gas delivery channels. While these designs decrease the overall pressure drop for a given flow rate of air for a specific plate area, the parallel channels are more prone to flooding as the presence of liquid water in one channel increases flow resistance in that channel, thereby diverting flow into other channels with relatively lower resistances. This is similar to the instabilities documented in parallel two-phase cooling channels, but without the effect of gas expansion during boiling.

In typical single serpentine channel designs, there is cross-talk between channels through the continuous GDL layer [34,35]. This cross-talk reduces the overall pressure drop in the channel and

Table 2
Experimental conditions for straight channels with equivalent fuel cell parameters.

i (A cm^{-2})	Q_w (μL min^{-1})	Q_w/inj. (μL min^{-1})	Q_a/std. (L min^{-1})			
			Stoich. coeff.			
			1	2	3	4
0.5	6.16	0.77	0.016	0.032	0.048	0.065
1	12.3	1.54	0.032	0.065	0.097	0.129
2	24.7	3.08	0.065	0.129	0.194	0.258

in the entire flow field. Cross-talk also creates zones at channel corners where water is easily trapped or accumulated as flow preferentially shortcuts the corner.

It is interesting to note that flooding of the channel is not observed under any flow conditions during the current studies, likely due to the single channel and sealed GDL configuration chosen for these tests. Where parallel channels provide alternative flow paths for the fluids, this single channel configuration and its larger pressure gradients and air velocities prevent blockage of the channels.

4. Summary and conclusions

As one component of the larger water management problem in PEM fuel cells, the design of gas delivery channels is in itself a complicated problem involving many competing phenomena.

In this study, an experimental system was developed to study two-phase flow in microchannels by ex situ visualization under known liquid and gas flow rates relevant to fuel cells in order to understand the flow conditions which favor particular flow structures in the channel. Images of the channels were collected along the length of the channel as the two-phase flow structure evolved. Flow structure labeling and mapping summarizes the observed flow regimes and the conditions under which they transition from one to another.

The geometric configuration of the channels has a significant effect on the local flow conditions. The gas flow rates are proportional to the entire length of the channel, while the liquid flow is "local", introduced along the length of the channel. This results in very different local ratios of liquid to gas flow rates depending on channel configuration and number of parallel flow channels.

In particular, the choice of the number of parallel flow channels covering the cell area has a marked effect on the flow conditions in those channels. The water flow in the channel depends on length of channel and reactions occurring under the upstream channels. The air flow rate for the cell is set based on the stoichiometry and the total reaction which will occur in the entire flow field. Along a channel, the ratio of water to air flow rate will vary from zero to the chosen stoichiometry along the length of the channel. This ratio changes more quickly in the case of multiple parallel channels because the channel lengths are shorter.

Multiple parallel channels reduce the overall pressure drop in the system for a given flow rate (stoichiometric ratio) or, in the case of a given pressure drop, allow more air flow through the channels. But the flow in multiple channels suffers from maldistribution, both inherent variations due to small geometric anomalies and induced redistribution due to the introduction of liquid water droplets [36,37]. These induced flow redistributions can create instabilities for the operation of the fuel cell microchannels. Gas flow is preferentially directed to channels which are not blocked by liquid water slugs, which can further aggravate the flow maldistribution.

Fewer parallel channels mean longer channel lengths. This allows for higher gas velocities in the channel, improving mass transport and enabling removal of water from the channels, but sustaining larger overall pressure drop and gas expansion in a given channel. However, fewer channels in parallel usually necessitate more corners as the channels serpentine to cover the reaction area. As the current study shows, corners trap liquid water and lead to liquid accumulation and film formation in the channels. The choice of channel configuration has a significant effect on the flow structures which occur in the channels.

The results of the current ex situ experiments provide insight into the effect of channel geometry and corners on the evolution of flow structures in long microchannels relevant to PEM fuel cell operation. It is observed that corners reduce the water-evacuation capability of the channels and facilitate the formation of liquid films on the walls of the channel. At the same time, water is more efficiently removed from the channels with the larger pressure gradient afforded by high air flow rates through long channels, rather than shorter parallel channels which can result in conditions prone to flooding. These results provide insight for gas delivery channels designed to optimize the performance of PEM fuel cells.

Acknowledgments

References

[1] X. Li, I. Sabir, J. Park, J. Power Sources 163 (2007) 933–942.
[2] F. Barbir, H. Gorgun, X. Wang, J. Power Sources 141 (2005) 96–101.
[3] S.W. Cha, R. O'Hayre, F.B. Prinz, Solid State Ionics 175 (2004) 789–795.
[4] T.V. Nguyen, M.W. Knobbe, J. Power Sources 114 (2003) 70–79.
[5] A. Bazylak, Int. J. Hydrogen Energy 34 (2009) 3845–3857.
[6] R. Anderson, L. Zhang, Y. Ding, M. Blanco, X. Bi, D.P. Wilkinson, J. Power Sources 195 (2010) 4531–4553.
[7] R. Satija, D.L. Jacobson, M. Arif, S.A. Werner, J. Power Sources 129 (2004) 238–245.
[8] D. Kramer, J. Zhang, R. Shimoi, E. Lehmann, A. Wokaun, K. Shinohara, G.G. Scherer, Electrochem. Acta 50 (2005) 2603–2614.
[9] N. Pekula, K. Heller, P.A. Chuang, A. Turhan, M.M. Mench, J.S. Brenizer, K. Unlu, Nucl. Instrum. Methods Phys. Res. A 21 (2005) 134.
[10] D.S. Hussey, D.L. Jacobson, M. Arif, J.P. Owejan, J.J. Gagliardo, T.A. Trabold, J. Power Sources 172 (2007) 225–228.
[11] T.A. Trabold, J.P. Owejan, D.L. Jacobson, M. Arif, P.R. Huffman, Int. J. Heat Mass Transfer 49 (2006) 4712–4720.
[12] S. Tsushima, K. Teranishi, S. Hirai, Electrochem. Solid State Lett. 7 (2004) A269–A272.
[13] P.K. Sinha, P. Halleck, C.-Y. Wang, Electrochem. Solid State Lett. 9 (2006) A344–A348.
[14] X. Liu, H. Guo, F. Ye, C.F. Ma, Electrochim. Acta 52 (2007) 3607–3614.
[15] H. Hakenjos, U. Muenter, C. Wittstadt, Hebling, J. Power Sources 131 (2004) 213–216.
[16] F.B. Weng, A. Su, C.Y. Hsu, Int. J. Hydrogen Energy 32 (2007) 666–676.
[17] K. Tuber, D. Pocza, C. Hebling, J. Power Sources 124 (2003) 403–414.
[18] X.G. Yang, F.Y. Zhang, A.L. Lubawy, C.Y. Wang, Electrochem. Solid State Lett. 7 (11) (2004) 408–411.
[19] D. Spernjak, A.K. Prasad, S.G. Advani, J. Power Sources 170 (2007) 334–344.
[20] D. Spernjak, S.G. Advani, A.K. Prasad, J. Electrochem. Soc. 156 (2009) B109–B117.
[21] T. Ous, C. Arcoumanis, J. Power Sources 173 (2007) 137–148.
[22] Z. Lu, S.G. Kandlikar, C. Rath, M. Grimm, W. Domigan, A.D. White, M. Hardbarger, J.P. Owejan, T.A. Trabold, Int. J. Hydrogen Energy 34 (2009) 3445–3456.
[23] L. Zhang, H.T. Bi, D.P. Wilkinson, J. Stumper, H. Wang, J. Power Sources 183 (2008) 643–650.

[24] A. Su, F.B. Weng, C.Y. Hsu, Y.M. Chen, Int. J. Hydrogen Energy 31 (2006) 1031–1039.
[25] J. Benziger, J. Nehlsen, D. Blackwell, T. Brennan, J. Itescu, J. Membr. Sci. 261 (2005) 98–106.
[26] J. Stumper, C. Stone, J. Power Sources 176 (2008) 468–476.
[27] M. Kawaji, P.M.-Y. Chung, Microscale Thermophys. Eng. 8 (2004) 239–257.
[28] I. Hassan, M. Vaillancourt, K. Pehlivan, Microscale Therm. Eng. 9 (2005) 165–182.
[29] R. Dreyfus, P. Tabeling, H. Willaime, Phys. Rev. Lett. 90 (1993), 144505-(1-4).
[30] K.A. Triplett, S.M. Ghiaasiaan, S.I. Abdel-Khalik, D.L. Sadowski, Int. J. Multiphase Flow 25 (1999) 377–394.
[31] J.L. Xu, P. Cheng, T.S. Zhao, Int. J. Multiphase Flow 25 (1999) 411–432.
[32] K. Pehlivan, I. Hassan, M. Vaillancourt, Appl. Therm. Eng. 26 (2006) 1506–1514.
[33] C.H. Hidrovo, F.-M. Wang, J.E. Steinbrenner, E.S. Lee, S. Vigneron, C.-H. Cheng, J.K. Eaton, K.E. Goodson, Proc. of ICMM, June 13–15, Toronto, Canada, 2005.
[34] J.P. Feser, A.K. Prasad, S.G. Advani, J. Fuel Cell Sci. Technol. 4 (2007) 328–335.
[35] J. Martin, P. Oshkai, N. Djilali, J. Fuel Cell Sci. Technol. 2 (2005) 70–80.
[36] A. Lozano, F. Barreras, L. Valino, C. Marin, Exp. Fluids 42 (2007) 301–310.
[37] F. Barreras, A. Lozano, L. Valino, C. Marin, A. Pascau, J. Power Sources 144 (2005) 54–66.